Nano Res
DOI 10.1007/s12274-010-0079-4
Research Article

ISSN 1998-0124
CN 11-5974/O4

A Facile One-Step Synthesis of TiO_2/Graphene Composites for Photodegradation of Methyl Orange

Haijiao Zhang[1], Panpan Xu[1], Guidong Du[1], Zhiwen Chen[1], Kokyo Oh[2], Dengyu Pan[1], and Zheng Jiao[1] (✉)

[1] Institute of Nanochemistry and Nanobiology, School of Environmental and Chemical Engineering, Shanghai University, Shanghai 200444, China
[2] Center for Environmental Science in Saitama, 914 Kamitanadare, Kazo, Saitama, Japan

Received: 26 August 2010 / Revised: 10 November 2010 / Accepted: 11 November 2010
© Tsinghua University Press and Springer-Verlag Berlin Heidelberg 2010

ABSTRACT

TiO_2/graphene composite photocatalysts have been prepared by a simple liquid phase deposition method using titanium tetrafluoride and electron beam (EB) irradiation-pretreated graphene as the raw materials. The products were characterized by X-ray diffraction, transmission electron microscopy, X-ray photoelectron spectroscopy, and thermogravimetric analysis. The effects of varying the synthesis parameters such as graphene content, concentration of titanium tetrafluoride solution and irradiation dose were investigated. It was found that the preparation conditions had a significant effect on the structure and properties of the final products. The irradiated graphene was covered with petal-like anatase TiO_2 nanoparticles, which were more uniform and smaller in size than those in products synthesized without EB irradiation-pretreated graphene. The photocatalytic activities of the products were evaluated using the photocatalytic degradation of methyl orange as a probe reaction. The results showed that the products synthesized using EB irradiation-pretreated graphene exhibited higher photocatalytic activities than those using graphene without EB irradiation pretreatment.

KEYWORDS

TiO_2/graphene composites, electron beam (EB) irradiation, photocatalytic degradation, methyl orange

1. Introduction

Titanium dioxide (TiO_2) is an important semiconductor, which is used in environmentally benign processes because of its advantageous properties such as non-toxicity, photo- and chemical stability, water insolubility under most conditions and low production cost [1, 2]. However, it is well known that the morphology and size of TiO_2 particles play very crucial roles in its properties and applications [1, 3]. To date, many synthesis methods have been developed in an attempt to improve the photocatalytic activity of powdered TiO_2 catalysts, including noble metal deposition, ion doping [4–7], and adding a co-adsorbent to TiO_2 [8–12]. Among these materials, multi-walled carbon nanotube (MWCNT)–TiO_2 composites have been studied extensively, and have proved to be very effective in improving the photocatalytic activity of TiO_2 [13–15].

Graphene, with its unique structure of one-atom-thick planar sheets of sp^2-bonded carbon atoms closely packed in a honeycomb crystal lattice, has attracted considerable attention due to its extraordinary mechanical and electronic properties [16–20]. Graphene

Address correspondence to zjiao@shu.edu.cn

can be viewed as split carbon nanotubes (CNTs), suggesting it has great potential to enhance the photocatalytic activity of catalysts like TiO_2 [13, 21]. Compared with CNTs, graphene has many advantages including high surface area (a theoretical value of 2630 m^2/g) [22] and good interfacial contact with adsorbates. Therefore, it is desirable to explore simple and effective approaches for synthesizing graphene-based composites and expand their applications. Very recently, there have been a few reports of the synthesis of TiO_2/graphene composites. For instance, TiO_2 particles and graphene oxide (GO) colloids have been mixed ultrasonically, followed by ultraviolet (UV)-assisted photocatalytic reduction of GO to yield TiO_2/graphene composites [23]. In another example, TiO_2/graphene composite materials were prepared by self-assembly of nanocrystalline TiO_2 grown in situ on graphene by a one-step approach with the assistance of an anionic surfactant [24]. There was another report on the use of titania P25–graphene composites as photocatalysts [25], in which the morphology of the composites remains to be optimized in order to achieve higher photocatalytic activity. Hence, it is still a great challenge to prepare TiO_2/graphene composites with the appropriate crystal structure to achieve high photocatalytic activity.

In this work, we describe a liquid phase deposition method for the preparation of TiO_2/graphene composites. The effect of electron beam (EB) irradiation of the graphene on the structure and properties of the materials was studied. As illustrated in Fig. 1, EB irradiation can arouse oxygenated groups on graphene surface. The carbon oxygen bands excited by EB irradiation on graphene surface can be considered as defect sites, which could increase the affinity of graphene to Ti^{4+} through electrostatic force, thus providing more growing spots for TiO_2 crystal. At the same time, the excited oxygenated groups were not very stable and could be partially reduced during the growth of TiO_2. The optimal experimental conditions were established by varying the reaction conditions. The photochemical degradation of methyl orange was employed as a probe reaction to determine the photocatalytic activity of the composites and their activities were compared with that of a mixture of P25 and graphene.

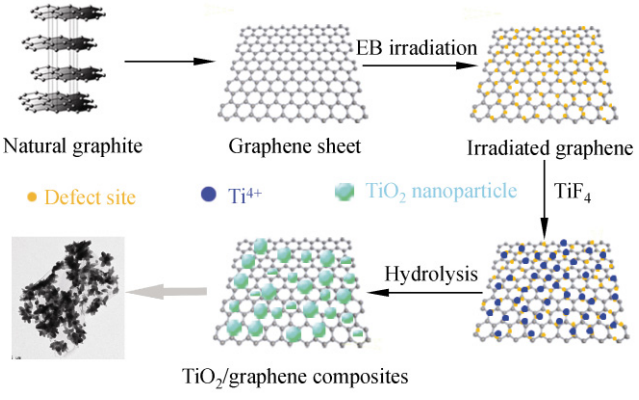

Figure 1 Diagram of the chemical route to the TiO_2/graphene composites

2. Experimental

2.1 Synthesis of TiO_2/graphene composites

Prior to the synthesis of TiO_2/graphene composites, GO was synthesized from natural graphite powder by a modified Hummers' method [26]. Then, as-synthesized GO was calcined at 500 ℃ for 2 h in a nitrogen atmosphere and the resulting powder was collected for use in the next step.

Typically, 20 mg of graphene prepared in the previous steps was added to 40 mL of 0.04 mol/L TiF_4 (from Acros Organics, Belgium) solution in a 200 mL glass beaker. The glass beaker was sealed with Parafilm and placed in an ultrasonic water bath for 50 min to ensure good dispersion of the graphene. The resulting mixture was then heated in an electric oven at 60 ℃ for 20 h. After reaction, the parafilm was found broken, due to the build-up pressure upon the reaction. The mixture was washed several times with deionized water and ethanol solution, and dried in an oven at 60 ℃ to obtain the final products.

Following the same procedure, a series of composite catalysts were prepared by varying the content of graphene and concentration of the TiF_4 solution.

In an attempt to improve the photocatalytic activity, EB irradiation was employed to irradiate the graphene before reaction. In a typical procedure, graphene was dispersed in aqueous solution, and then the mixture was placed in a polythene bag and irradiated under the electron beam of an accelerator with a

dose of 2.1×10^5 Gy and a current of 7.0 mA. With all other experimental conditions being kept the same, experiments were also carried out by varying the dose of EB irradiation on graphene.

2.2 Catalyst characterization

Samples were characterized by X-ray diffraction (XRD, Rigaku D/max-2550, Cu Kα radiation), ultraviolet and visible spectroscopy (UV–vis, U-3010), transmission electron microscopy (TEM, JSM-2010F) and high-resolution transmission electron microscopy (HRTEM, JSM-2010F). Raman spectra of samples were recorded using a Renishaw inVia system with an excitation wavelength of 785 nm and a charge-coupled device detector. Thermogravimetric (TG) and differential thermogravimetric (DTG) analysis was carried out with a STA 409 PC/4/H Luxx system using a heating rate of 10 ℃/min in a flow of air. N_2 adsorption–desorption isotherms were measured on a QUADRASORB SI Surface Area and Pore Size Analyzer at 77 K using the volumetric method, after the as-prepared samples were annealed at 200 ℃. The Brunauer–Emmett–Teller (BET) specific surface area was calculated by using adsorption data. Atomic force microscopy (AFM) images were obtained by using a SPM-9600 instrument (Shimadzu, Japan). The substrates used for AFM imaging were freshly cleaved mica substrates. X-ray photoelectron spectroscopy (XPS) measurements were performed on an AXIS Ultra DLD (Kratos, USA) using monochromatic Al Kα X-ray source (anode HT = 15 kV) operating at a vacuum better than 10^{-7} Pa. Kratos Vision v. 2.2 software was utilized to analyze and deconvolute the XPS peaks.

2.3 Photodegradation reactions

The photocatalytic activity of TiO_2/graphene composites was evaluated using methyl orange degradation in aqueous solution under UV light irradiation. Experiments were carried out in an SGY-IB photochemical reactor. Typically, 20 mg of as-prepared TiO_2/graphene composite catalyst was added to 50 mL of 0.025 g/L methyl orange solution in a 100 mL beaker. The mixture was then placed in an ultrasonic water bath for 30 min to ensure good dispersion of the catalyst, followed by stirring in the dark at ambient temperature for 1 h to achieve adsorption–desorption equilibrium for methyl orange. After reaching equilibrium, 3–5 mL of suspension was extracted in order to determine the initial concentration of methyl orange solution, which was recorded as the base concentration C_0. The remaining mixture was transferred to a 50 mL quartz tube and illuminated with a 300 W Hg lamp. In the following 60 min, 3–5 mL aliquots of the suspension were removed every 10 min. The suspension was centrifuged immediately to separate any suspended solid. The UV–vis spectra of the supernatant were recorded using a Hitachi U-3010 UV–vis spectrophotometer to determine the concentration of methyl orange at each time, which is denoted as C_t. For comparison, a mixture of P25 and irradiated/unirradiated graphene (the amount of TiO_2 was kept the same as in the composites) and bare graphene (20 mg) were employed under the same conditions.

3. Results and discussion

3.1 Characterization of GO and graphene sheets

As shown in Fig. S-1 in the ESM, the thickness of the GO layer was 1.32 nm, larger than the typical thickness of single-layer GO (~0.8 nm), but still smaller than the typical thickness of a bilayer graphene, indicating that single-layer graphene accounted for the major part of the prepared materials [27]. In addition, as calcination at 500 ℃ in an N_2 atmosphere does not result in restacking of GO sheets, it can be deduced that the graphene used in this study is mostly single-layer graphene.

XPS was employed to study the chemical states of the prepared samples. The peak deconvolution of the C (1s) XPS core level of GO sheets and graphene sheets reduced by annealing at 500 ℃ are shown in Fig. S-2 in the ESM. Peaks with binding energies of 284.6 eV and 285.4 eV can be attributed to the C–C and C (CH_2) bonds, respectively. The deconvoluted peaks centered at binding energies of 286.2 and 288.1 eV can be assigned to C–OH and C=O functional groups, respectively [27–30]. Before the annealing treatment, considerable contributions from the oxygen-containing functional groups were observed. After annealing

treatment, however, the areas of these peaks decreased considerably due to the reduction process. The peak area ratios of the C–OH and C=O bonds to the C–C bonds are summarized in Table S-1 in the ESM. The relative concentrations of the C–OH and C=O bonds showed decreases of 73% and 78% from the corresponding concentrations for the GO sheets. This indicates that an effective, but not complete, chemical reduction of the GO sheets to graphene has occurred. The residual small amount of oxygen-containing bonds should not significantly affect the properties of the graphene, however.

3.2 Effect of the graphene content

The effect of graphene on the catalytic activity of the prepared composite catalyst was studied by varying the content of graphene while keeping the other conditions constant. Figure 2 presents the XRD patterns of the catalysts when the graphene dose was 10 (a), 20 (b), 30 (c), and 40 mg (d). It can be observed that a pure anatase TiO_2 phase (JCPDS No. 21-1272) was obtained for a graphene content of 20 mg. For other graphene contents, additional peaks from impurities such as TiOF and $TiOF_2$ appeared (marked with symbols "*" and "#", respectively). As illustrated in the experimental section, a parafilm was used to seal the beaker during the reaction. And the as-prepared samples under our experimental condition have more uniform morphology compared with that prepared under completely closed or open condition (data not shown), corresponding to the present literature report [15]. The TiO_2/graphene composites were obtained from the hydrolysis of TiF_4 in the presence of aqueous dispersions of graphene, as shown in eq 1.

$$TiF_4 + \text{graphene} + 2H_2O \cdot TiO_2/\text{graphene(s)} + 4HF \quad (1)$$

It has been reported that the hydrolysis reaction to form TiO_2 rely on the content of the graphene [31]. When 10 mg graphene was suspended in the system, the reaction rate was slow, with the reaction progressing, a part of water evaporated and large amount of residual TiF_4 would form high concentration TiF_4 solution, leading to formation of TiOF and $TiOF_2$ impurities. While at high graphene content (30 mg, 40 mg), the initial reaction rate was so fast that the parafilm was soon broken by generated HF gas, then the water would evaporated fast and high concentration TiF_4 solution would form, also leading to TiOF and $TiOF_2$ impurities. In addition, it is worth mentioning that the TiOF and $TiOF_2$ impurities were transformed to anatase TiO_2 after calcination at 300 ℃ for 2 h. However, since calcination would increase the particle size of TiO_2 and hence decrease its photocatalytic activity, all the samples used in our work were obtained without calcination.

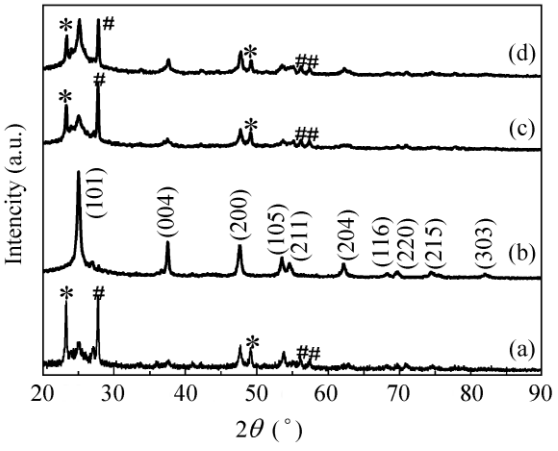

Figure 2 XRD patterns of TiO_2/graphene composites synthesized with different graphene contents (a) 10 mg, (b) 20 mg, (c) 30 mg, and (d) 40 mg

Figure 3 shows the Raman spectra of TiO_2/graphene composites prepared with 20 mg of graphene and 0.04 mol/L TiF_4 solution. A well resolved TiO_2 Raman

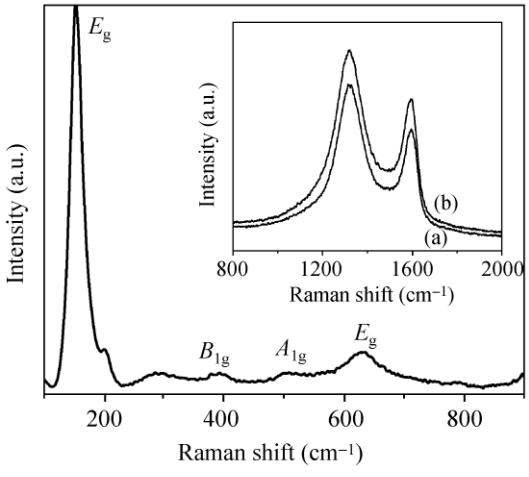

Figure 3 Raman spectra of the TiO_2/graphene composite prepared with 20 mg of graphene and 0.04 mol/L TiF_4 solution. The inset shows Raman spectra (800 to 2000 cm^{-1}) of (a) the TiO_2/graphene composite and (b) pure graphene

peak is clearly seen at about 153 cm^{-1}, which is attributed to the main E_g anatase vibration mode. Furthermore, vibration peaks at 400 cm^{-1} (B_{1g}), 517 cm^{-1} (A_{1g}) and 640 cm^{-1} (E_g) are also characteristic of anatase TiO_2 [32].

The Raman spectra are therefore consistent with the XRD results shown in Fig. 2(b). Additionally, two peaks at about 1320 cm^{-1} (D band) and 1594 cm^{-1} (G band) are observed in the spectra (see the inset in Fig. 3), which can be attributed to the graphene substrate. The intensity ratios (I_D/I_G) for bare graphene and the TiO_2/graphene composite were 2.31 and 2.02, respectively. The decrease in the D/G intensity ratio for the TiO_2/graphene composite suggests that a decrease in the average size of the sp^2 domains of C atoms took place during the growth of anatase crystallites [33].

Figure 4 displays the TG and DTG curves of as-prepared graphene and the TiO_2/graphene composite prepared with 20 mg of graphene and 0.04 mol/L TiF_4 solution. As shown in Fig. 4(a), the pure graphene decomposed completely on heatingin air below 900 ℃. The DTG curve exhibits strong bands centered at about 687 ℃, which correspond to the gasification of graphene. In Fig. 4(b), the TG curve of the TiO_2/graphene composite shows a small mass loss of 12% and a larger mass loss of 25%, which can be attributed to water removal and structural water evolution, and graphene gasification, respectively. In the DTG curve, the temperature at which the maximum rate of graphene gasification occurs is about 685 ℃, which is consistent with that of pure graphene.

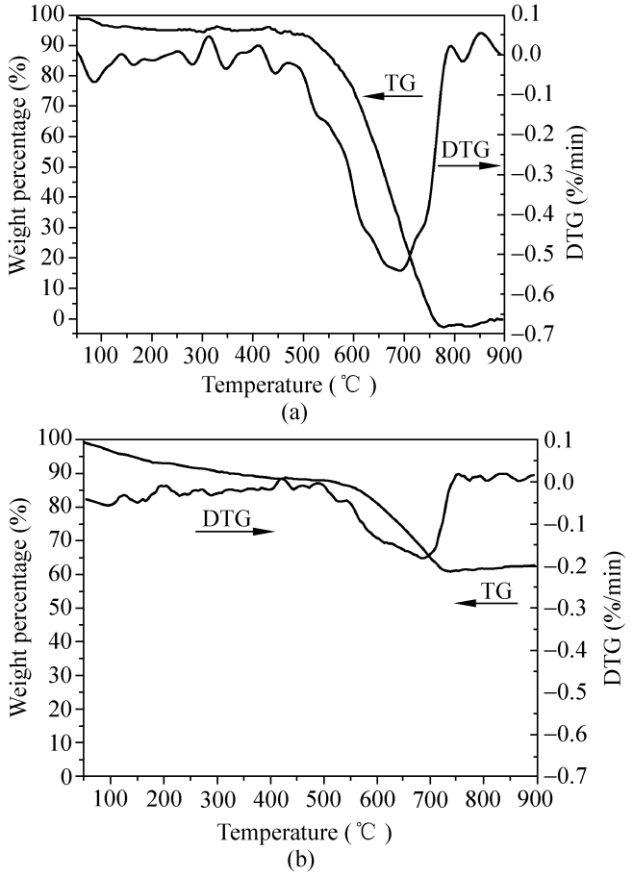

Figure 4 TG and DTG curves of (a) pure graphene and (b) the TiO_2/graphene composite prepared with 20 mg of graphene and 0.04 mol/L TiF_4 solution

In Fig. 5(a), C (1s) for TiO_2/graphene composites prepared with 20 mg of graphene and 0.04 mol/L TiF_4

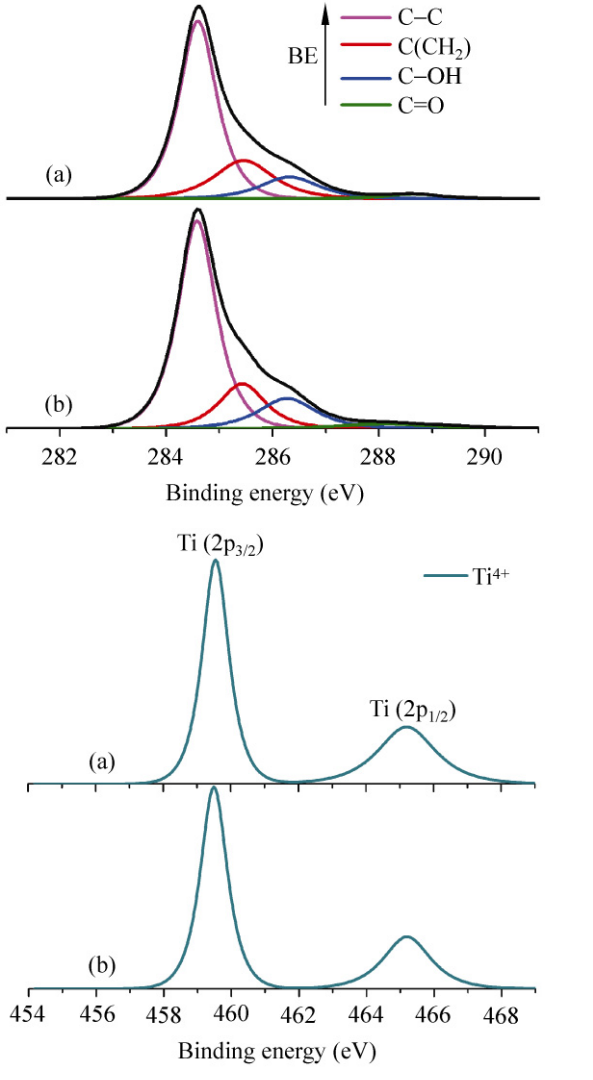

Figure 5 Peak deconvolution of C (1s) and Ti (2p) XPS core levels of (a) a TiO_2/graphene composite prepared with 20 mg of graphene and 0.04 mol/L TiF_4 solution and (b) the TiO_2/graphene composite synthesized with 2.1×10^5 Gy irradiation

solution showed similar peak deconvolution results with that of annealing graphene. But as displayed in Table 1, a slightly increase in the peak area (A) ratios of the oxygen-containing bonds to the CC bonds was observed compared with that of bare graphene sheets. The reason may be that upon growth of TiO_2 on graphene surface, the concentration of the CC bonds may decrease slightly. The XPS spectrum at the Ti (2p) binding energy region was also present in Fig. 5 (b). The two bands located at binding energies of 465.2 and 459.5 eV were assigned to the Ti ($2p_{1/2}$) and Ti ($2p_{3/2}$) spin-orbital splitting photoelectrons in the Ti^{4+} chemical state, respectively. A 5.7 eV peak-to-peak separation indicated the formation of TiO_2 on graphene surface [34, 35].

3.3 Effect of the TiF_4 concentration

The concentration of TiF_4 was varied while the content of graphene was kept constant at 20 mg. Figure 6 shows XRD patterns of the samples when the TiF_4 concentration was 0.02 (a), 0.04 (b), 0.06 (c), and 0.08 mol/L (d). For a concentration of TiF_4 of 0.08 mol/L, the sample appeared to contain TiOF and $TiOF_2$ impurities. The characteristic peaks of TiOF and $TiOF_2$ are marked with the symbols "*" and "#", respectively. As shown in the TEM images (Fig. 7), the growth of petal-like TiO_2 on graphene increases gradually with the increasing TiF_4 concentration.

Figure 8 presents the results of photodegradation reactions of methyl orange solution. As the pure TiO_2 nanoparticles prepared using the same procedure in

Table 1 The peak area (A) ratios of the oxygen-containing bonds to the C–C bonds, for composites with and without irradiation

Irradiation dose	0 Gy	2.1×10^5 Gy
A_{COH}/A_{CC}	0.19	0.21
A_{CO}/A_{CC}	0.04	0.05

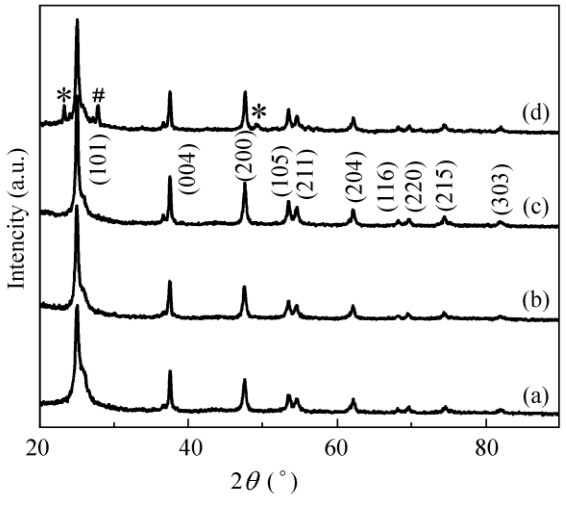

Figure 6 XRD patterns of TiO_2/graphene composites synthesized with different TiF_4 concentrations of (a) 0.02 mol/L, (b) 0.04 mol/L, (c) 0.06 mol/L, and (d) 0.08 mol/L

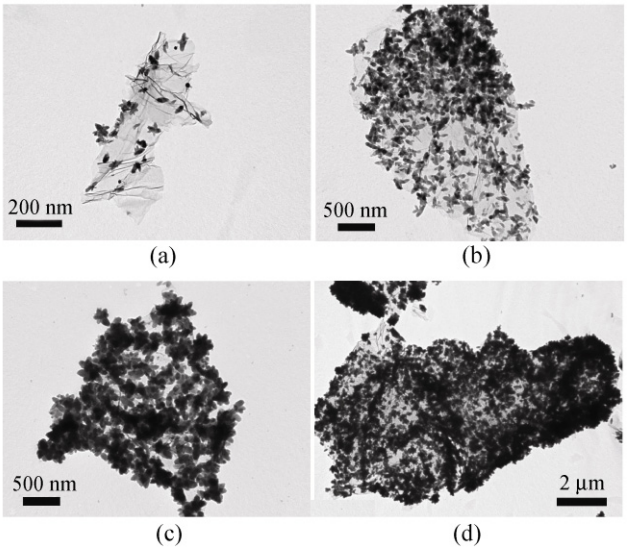

Figure 7 TEM images of TiO_2/graphene composites synthesized with different TiF_4 concentrations of (a) 0.02 mol/L, (b) 0.04 mol/L, (c) 0.06 mol/L, and (d) 0.08 mol/L

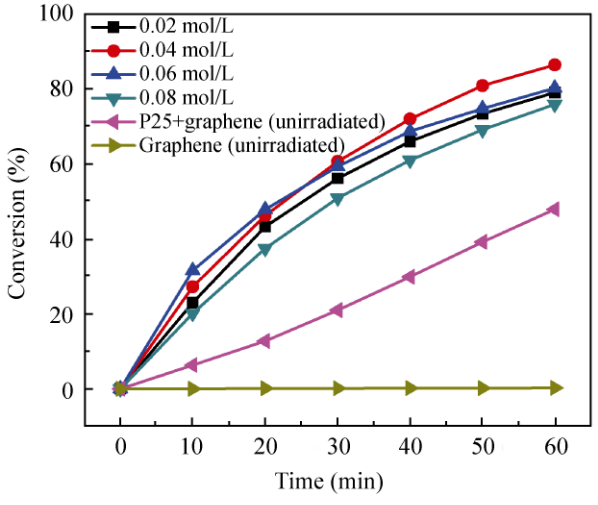

Figure 8 Conversion of methyl orange in photodegradation over TiO_2/graphene composites synthesized with different TiF_4 concentration, together with the results for a mixture of P25 and graphene, and bare unirradiated graphene for comparison

the absence of graphene tended to agglomerate into bulk and exhibited very low photocatalytic efficiency, P25 (a commercial photocatalyst) and unirradiated graphene were used as comparison materials to evaluate photocatalytic activity of TiO_2/graphene composites. As shown in Fig. 8, bare unirradiated graphene did not demonstrate any photocatalytic activity. The TiO_2/graphene composite catalyst with the best performance appeared to be the one synthesized with 0.04 mol/L TiF_4 solution. The conversion of methyl orange was about 85% after UV light irradiation for 60 min, which is much higher than that of a mixture of P25 and graphene.

3.4 Effect of the irradiation dose

EB irradiation was used for pretreatment of graphene in our work. Various dosages of EB irradiation were employed whilst keeping the other conditions unchanged (including a content of graphene of 20 mg and a TiF_4 concentration of 0.04 mol/L). Figure 9 shows the XRD patterns of as-prepared TiO_2/graphene composites when the irradiation dose was 7×10^4 (a), 1.4×10^5 (b), 2.1×10^5 (c), and 2.8×10^5 Gy (d). These XRD patterns appear identical to those in Fig. 6, indicating that EB irradiation did not alter the TiO_2 anatase structure. TEM images of the corresponding samples are shown in Fig. 10. The TiO_2 cluster size

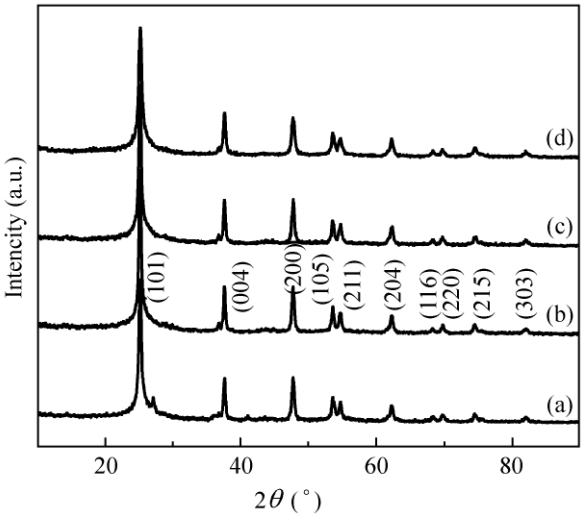

Figure 9 XRD patterns of TiO_2/graphene composites synthesized with different irradiation doses of (a) 7×10^4 Gy, (b) 1.4×10^5 Gy, (c) 2.1×10^5 Gy, and (d) 2.8×10^5 Gy

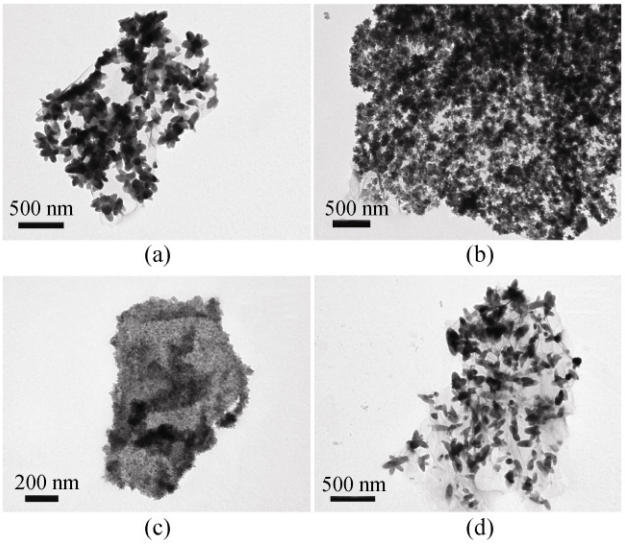

Figure 10 TEM images of TiO_2/graphene composites synthesized with different irradiation doses of (a) 7×10^4 Gy, (b) 1.4×10^5 Gy, (c) 2.1×10^5 Gy, and (d) 2.8×10^5 Gy

decreased when the EB irradiation dose was increased from 7×10^4 to 2.1×10^5 Gy. However, when the EB irradiation dose was increased to 2.8×10^5 Gy, the TiO_2 crystal cluster size increased compared to that of 2.1×10^5 Gy. To further explore the effect of EB irradiation, HRTEM was employed for sample characterization. As shown in Fig. 11, in both cases with and without EB irradiation, the petal-like structures of TiO_2 grown on graphene are composed of numerous tiny TiO_2 crystallites. However, the crystal cluster size of the samples prepared with EB irradiation pretreatment (Figs. 11(c) and 11(d)) appear to be smaller and more uniformly distributed than those in samples prepared without EB irradiation (Figs. 11(a) and 11(b)). In addition, N_2 adsorption–desorption isotherms were also employed to determine the specific surface area of prepared samples. The calculated BET surface areas of materials produced with and without EB irradiation pretreatment were 175.7 and 51.7 m^2/g, respectively. The corresponding total pore volumes were 0.28 and 0.11 cm^3/g, respectively. These results show that 2.1×10^5 Gy of irradiation can reduce crystallite cluster size and increase BET surface area of the TiO_2/graphene composites, both of which changes which should enhance the photocatalytic activity of the materials in the degradation of methyl orange solution.

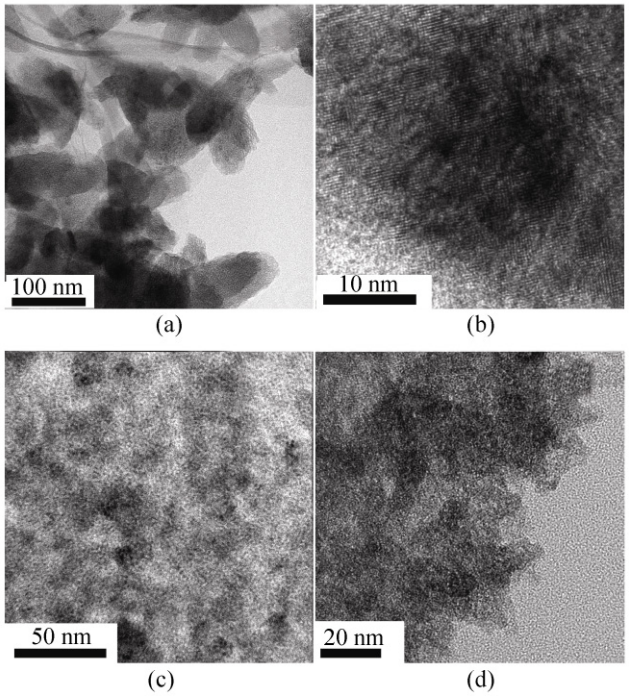

Figure 11 HRTEM images of TiO_2/graphene composites synthesized (a, b) without EB irradiation pretreatment, and (c, d) with EB irradiation pretreatment of 2.1×10^5 Gy

To explain the effect of EB irradiation, XPS spectra and peak area (*A*) ratios of the oxygen-containing bonds to the CC bonds for graphene irradiated with different irradiation dose were present in Fig. S-3 and Table S-2 in the ESM, respectively. The results showed that when the EB irradiation dose increased from 7×10^4 to 2.1×10^5 Gy, the peak area ratios of the C–OH and C=O bonds to the C–C bonds increased gradually. While when the dose was increased to 2.8×10^5 Gy, ACOH, AOH as well as Acc decreased greatly compared with that of unirradiated graphene, indicating the damage in lattice structure of graphene. The results are consistent with present reports [36, 37]. The carbon oxygen bands excited by EB irradiation on graphene surface can be considered as defect sites, which could increase the affinity of graphene to Ti^{4+} through electrostatic force, thus providing more growing spots for TiO_2 crystal. With the growing of TiO_2 crystal, the steric hindrance could affect the morphology of TiO_2 growing on the surface of graphene. And more defect sites lead to smaller TiO_2 cluster size. Herein, the TiO_2 cluster size decreased when the EB irradiation dose was increased from 7×10^4 to 2.1×10^5 Gy.

The deconvoluted C (1s) and Ti (2p) XPS spectra of the TiO_2/graphene composite synthesized with 2.1×10^5 Gy irradiation are shown in Figs. 5(a) and 5(b). They are consistent with that of composites synthesized without irradiation. Seen from Table 1, only a slightly increase in ratios of the C–OH and C=O bonds was observed, which indicated that the excited oxygenated groups by EB irradiation were not very stable and could be partially reduced during the growth of TiO_2. Herein, though the EB irradiation would increase the oxygenated groups on graphene, the properties of graphene in the prepared TiO_2/graphene composites would not be greatly affected.

Figure 12 displays the catalytic performance in photodegradation reactions of the catalysts prepared with different doses of EB irradiation. Bare 2.1×10^5 Gy EB irradiated graphene did not exhibit any photocatalytic activity, and the mixture of irradiated graphene and P25 demonstrated no obvious increase in photocatalytic efficiency in comparison with that of the mixture without irradiation. The TiO_2/graphene composite prepared with 2.1×10^5 Gy of EB irradiation showed the best catalytic performance. This indicates that EB irradiation pretreatment can lead to a beneficial morphological change in the catalyst resulting in an enhancement of photocatalytic activity. In particular,

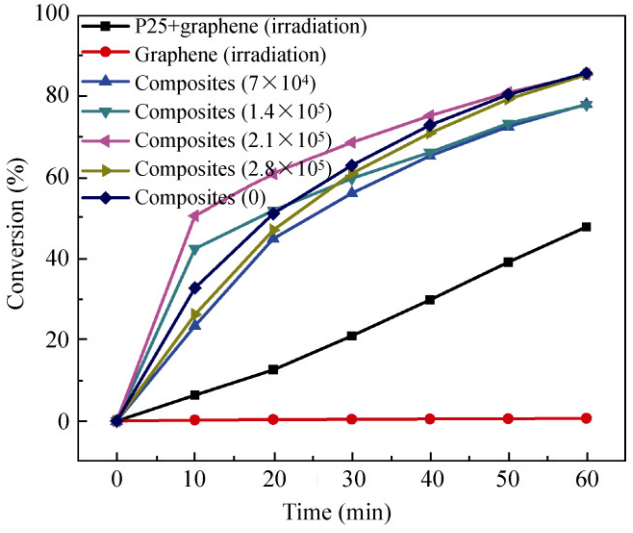

Figure 12 Conversion of methyl orange in photodegradation using TiO_2/graphene composite catalysts synthesized with different irradiation doses, with the results for a mixture of P25 and 2.1×10^5 Gy irradiated graphene, and bare irradiated graphene for comparison

it appeared that the photocatalytic activity of samples increased with increasing EB irradiation dosage in the order $2.1 \times 10^5 > 1.4 \times 10^5 > 2.8 \times 10^5 > 7 \times 10^4$ Gy.

Based on the comparison of TEM images, it can be concluded that the photocatalytic activity of the composites increased with decreasing TiO_2 crystal cluster size. The reason may be that decreasing the TiO_2 crystal cluster size results in an increase in contact area between the catalyst and organic molecules, which favors the degradation of methyl orange.

4. Conclusions

In summary, the TiO_2/graphene composite catalysts were prepared using a facial one-stepn easy and environmentally benign method. Key synthesis parameters such as the graphene content, concentration of TiF_4 solution and EB irradiation dose were optimized in our experiments. The TEM results showed that EB irradiation pretreatment of graphene is an effective way to produce uniform and small size TiO_2 nanoparticles on graphene. More importantly, the photodegradation results confirmed that EB irradiation pretreatment of graphene could significantly enhance the photocatalytic activity of TiO_2 in the degradation of methyl orange. Certainly, however, further improvements in photocatalytic performance of TiO_2/graphene composites are needed in order to develop practical applications in the environmental field.

Acknowledgements

The work was co-supported by the National Natural Science Foundation of China (No. 20871081), the Science and Technology Commission of Shanghai Municipality (Nos. 10QH1401000, and 10DZ0500100), the Research Funding of the State Key Laboratory of Chemical Engineering (ECUST), the Shanghai Key Laboratory of Green Chemistry and Chemical Processes, Department of Chemistry (ECNU), and Shanghai Leading Academic Disciplines (No. S30109).

Electronic Supplementary Material: Supplementary material (AFM image of GO, XPS spectra of GO, unirradiated graphene and irradiated grapheme, Table of peak area (A) ratios of the oxygen-containing bonds to the CC bonds for GO and EB irradiated graphene) is available in the online version of this article at http://dx.doi.org/10.1007/s12274-010-0079-4.

References

[1] Hoffmann, M. R.; Martin, S. T.; Choi, W.; Bahnemannt, D. W. Environmental applications of semiconductor photocatalysts. *Chem. Rev.* **1995**, *95*, 69–96.

[2] Fukahori, S.; Ichiura, H.; Kitaoka, T.; Tanaka, H. Photocatalytic decomposition of bisphenol A in water using composite TiO_2–zeolite sheets prepared by a papermaking technique. *Environ. Sci. Technol.* **2003**, *37*, 1048–1051.

[3] Fujishima, A.; Rao, T. N.; Tryk, D. A. Titanium dioxide photocatalysis. *J. Photochem. Photobiol. C: Photochem. Rev.* **2000**, *1*, 1–21.

[4] Chen, C.; Li, X.; Ma, W.; Zhao, J.; Hidaka, H.; Serpone, N. Effect of transition metal ions on the TiO_2-assisted photodegradation of dyes under visible irradiation: A probe for the interfacial electron transfer process and reaction mechanism. *J. Phys. Chem. B* **2002**, *106*, 318–324.

[5] Paola, A. D.; Marci, G.; Palmisano, L.; Schiavello, M.; Uosaki, K.; Ikeda, S.; Ohtani, B. Preparation of polycrystalline TiO_2 photocatalysts impregnated with various transition metal ions: Characterization and photocatalytic activity for the degradation of 4-nitrophenol. *J. Phys. Chem. B* **2002**, *106*, 637–645.

[6] Yu, J. C.; Yu, J.; Ho, W.; Jiang, Z.; Zhang, L. Effects of F-doping on the photocatalytic activity and microstructures of nanocrystalline TiO_2 powders. *Chem. Mater.* **2002**, *14*, 3808–3816.

[7] Mu, W.; Herrmann, J. M.; Pichat, P. Room temperature photocatalytic oxidation of liquid cyclohexane into cyclohexanone over neat and modified TiO_2. *Catal. Lett.* **1989**, *3*, 73–84.

[8] Robert, D.; Piscopo, A.; Heintz, O.; Weber, J. V. Photocatalytic detoxification with TiO_2 supported on glass-fibre by using artificial and natural light. *Catal. Today* **1999**, *54*, 291–296.

[9] Fernández, A.; Lassaletta, G.; Jiménez, V. M.; Justo, A.; González-Elipe, A. R.; Herrmann, J. -M.; Tahiri, H.; Ait-Ichou, Y. Preparation and characterization of TiO_2 photocatalysts supported on various rigid supports (glass, quartz and stainless steel). Comparative studies of photocatalytic activity in water purification. *Appl. Catal. B: Environ.* **1995**, *7*, 49–63.

[10] Minero, C.; Catozzo, F.; Pelizzetti, E. Role of adsorption in photocatalyzed reactions of organic molecules in aqueous titania suspensions. *Langmuir* **1992**, *8*, 481–486.

[11] Takeda, N.; Torimoto, T.; Sampath, S.; Kuwabata, S.; Yoneyama, H. Effect of inert supports for titanium dioxide loading on enhancement of photodecomposition rate of gaseous propionaldehyde. *J. Phys. Chem.* **1995**, *99*, 9986–9991.

[12] Tanguay, J. F.; Suib, S. L.; Coughlin, R. W. Dichloromethane photodegradation using titanium catalysts. *J. Catal.* **1989**, *117*, 335–347.

[13] Woan, K.; Pyrgiotakis, G.; Sigmund, W. Photocatalytic carbon-nanotube–TiO_2 composites. *Adv. Mater.* **2009**, *21*, 2233–2239.

[14] Yu, Y.; Yu, J. C.; Yu, J. G.; Kwok, Y. C.; Che, Y. K.; Zhao, J. C.; Ding, L.; Ge, W. -K.; Wong, P.-K. Enhancement of photocatalytic activity of mesoporous TiO_2 by using carbon nanotubes. *Appl. Catal. A: Gen.* **2005**, *289*, 186–189.

[15] Liu, B.; Zeng, H. C. Carbon nanotubes supported mesoporous mesocrystals of anatase TiO_2. *Chem. Mater.* **2008**, *20*, 2711–2719.

[16] Geim, A. K.; Novoselov, K. S. The rise of graphene. *Nat. Mater.* **2007**, *6*, 183–191.

[17] Meyer, J. C.; Geim, A. K.; Katsnelson, M. I.; Novoselov, K. S.; Booth, T. J.; Roth, S. The structure of suspended graphene sheets. *Nature* **2007**, *446*, 60–63.

[18] Charlier, J. C.; Eklund, P. C.; Zhu, J.; Ferrari, A. C. Electron and phonon properties of graphene: Their relationship with carbon nanotubes. In *Topics in Applied Physics;* Jorio, A.; Dresselhaus, G.; Dresselhaus, M. S., Eds.; Springer: Berlin (Heidelberg), 2008; pp. 673–709.

[19] Barone, V.; Hod, O.; Scuseria, G. E. Electronic structure and stability of semiconducting graphene nanoribbons. *Nano Lett.* **2006**, *6*, 2748–2754.

[20] Frank, I. W.; Tanenbaum, D. M.; van der Zande, A. M.; McEuen, P. L. Mechanical properties of suspended graphene sheets. *J. Vac. Sci. Technol. B* **2007**, *25*, 2558–2561.

[21] Akturk, A.; Goldsman, N. Electron transport and full-band electron–phonon interactions in graphene. *J. Appl. Phys.* **2008**, *103*, 053702.

[22] Peigney, A.; Laurent, C.; Flahaut, E.; Bacsa, R. R.; Rousset, A. Specific surface area of carbon nanotubes and bundles of carbon nanotubes. *Carbon* **2001**, *39*, 507–514.

[23] Williams, G.; Seger, B.; Kamat, P. V. TiO_2–graphene nanocomposites. UV-assisted photocatalytic reduction of graphene oxide. *ACS Nano* **2008**, *2*, 1487–1491.

[24] Wang, D.; Choi, D.; Li, J.; Yang, Z.; Nie, Z.; Kou, R.; Hu, D.; Wang, C.; Saraf, L. V.; Zhang, J.; Aksay, I. A.; Liu, J. Self-assembled TiO_2–graphene hybrid nanostructures for enhanced Li-ion insertion. *ACS Nano* **2009**, *3*, 907–914.

[25] Zhang, H.; Lv, X. J.; Li, Y. M.; Wang, Y.; Li, J. H. P25–graphene composite as a high performance photocatalyst. *ACS Nano* **2010**, *4*, 380–386.

[26] Xu, Y. X.; Bai, H.; Lu, G. W.; Li, C.; Shi, G. Q. Flexible graphene films via the filtration of water-soluble noncovalent functionalized graphene sheets. *J. Am. Chem. Soc.* **2008**, *130*, 5856–5857.

[27] Akhavan, O. The effect of heat treatment on formation of graphene thin films from graphene oxide nanosheets. *Carbon* **2010**, *48*, 509–519

[28] Yang, D. X.; Velamakanni, A.; Bozoklu, G.; Park, S.; Stoller, M.; Piner, R. D. Chemical analysis of graphene oxide films after heat and chemical treatments by X-ray photoelectron and micro-Raman spectroscopy. *Carbon* **2009**, *47*, 145–152.

[29] Akhavan, O. Photocatalytic reduction of graphene oxides hybridized by ZnO nanoparticles in ethanol. *Carbon* **2011**, *49*, 11–18.

[30] Akhavan, O. Graphene nanomesh by ZnO nanorod photocatalysts. *ACS Nano* **2010**, *4*, 4174–4180.

[31] Lambert, T. N.; Chavez, C. A.; Hernandez-Sanchez, B.; Lu, P.; Bell, N. S.; Ambrosini, A. Synthesis and characterization of titania-graphene nanocomposites. *J. Phys. Chem. C* **2009**, *113*, 19812–19823.

[32] Falaras, P.; Hugot-Le Goff, A.; Bernard, M. C.; Xagas, A. Characterization by resonance Raman spectroscopy of sol–gel TiO_2 films sensitized by the $Ru(PPh_3)_2(dcbipy)Cl_2$ complex for solar cells application. *Sol. Energy Mater. Sol. Cells* **2000**, *64*, 167–182.

[33] Tuinstra, F.; Koenig, J. L. Raman spectrum of graphite. *J. Chem. Phys.* **1970**, *53*, 1126–1130.

[34] Akhavan, O.; Ghaderi, E. Photocatalytic reduction of graphene oxide nanosheets on TiO_2 thin film for photoinactivation of bacteria in solar light irradiation. *J. Phys. Chem. C* **2009**, *113*, 20214–20220.

[35] Akhavan, O.; Abdolahad, M.; Esfandiar, A.; Mohatashamifar, M. Photodegradation of graphene oxide sheets by TiO_2 nanoparticles after a photocatalytic reduction. *J. Phys. Chem. C* **2010**, *114*, 12955–12959.

[36] Teweldebrhan, D.; Balandin, A. A. Modification of graphene properties due to electron-beam irradiation. *Appl. Phys. Lett.* **2009**, *94,* 013101.

[37] Kim, K.; Choi, J.; Lee, H.; Lee, H. K.; Kang, T. H.; Han, Y. H.; Lee. B. C.; Kim, S.; Kim, B. Effects of 1 MeV electron beam irradiation on multilayer graphene grown on 6H-SiC(0001). *J. Phys. Chem. C* **2008**, *112*, 13062–13064.

Table of contents

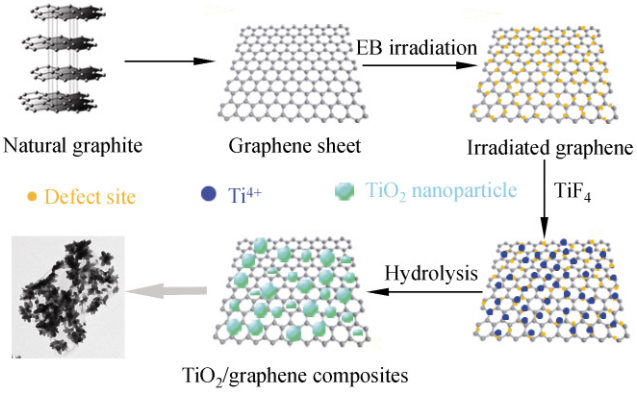

TiO_2/graphene composite photocatalysts have been prepared by a simple liquid phase deposition method using titanium tetrafluoride and electron beam (EB) irradiation-pretreated graphene as the raw materials, and their photocatalytic properties studied.

Electronic Supplementary Material

A Facile One-Step Synthesis of TiO_2/Graphene Composites for Photodegradation of Methyl Orange

Haijiao Zhang[1], Panpan Xu[1], Guidong Du[1], Zhiwen Chen[1], Kokyo Oh[2], Dengyu Pan[1], and Zheng Jiao[1] (✉)

[1] Institute of Nanochemistry and Nanobiology, School of Environmental and Chemical Engineering, Shanghai University, Shanghai 200444, China

[2] Center for Environmental Science in Saitama, 914 Kamitanadare, Kazo, Saitama, Japan

Supporting information to DOI 10.1007/s12274-010-0079-4

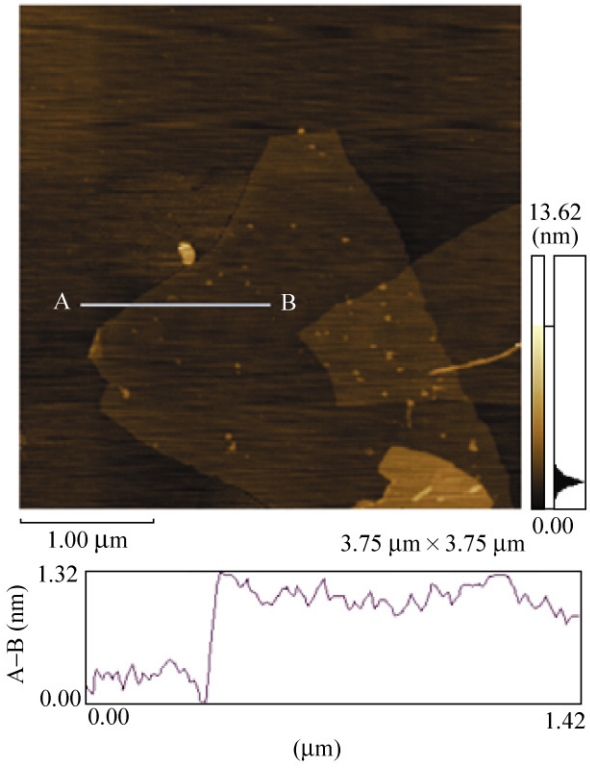

Figure S-1 AFM image of as-prepared GO sheets

Address correspondence to zjiao@shu.edu.cn

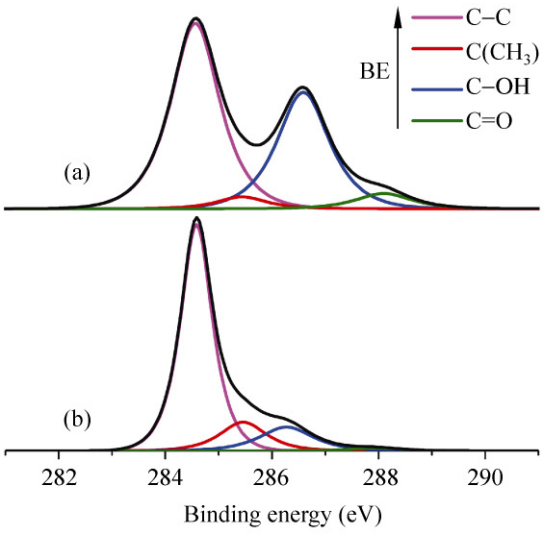

Figure S-2 Peak deconvolution of the C (1s) XPS core level of (a) GO sheets and (b) graphene sheets reduced by annealing at 500 ˚C

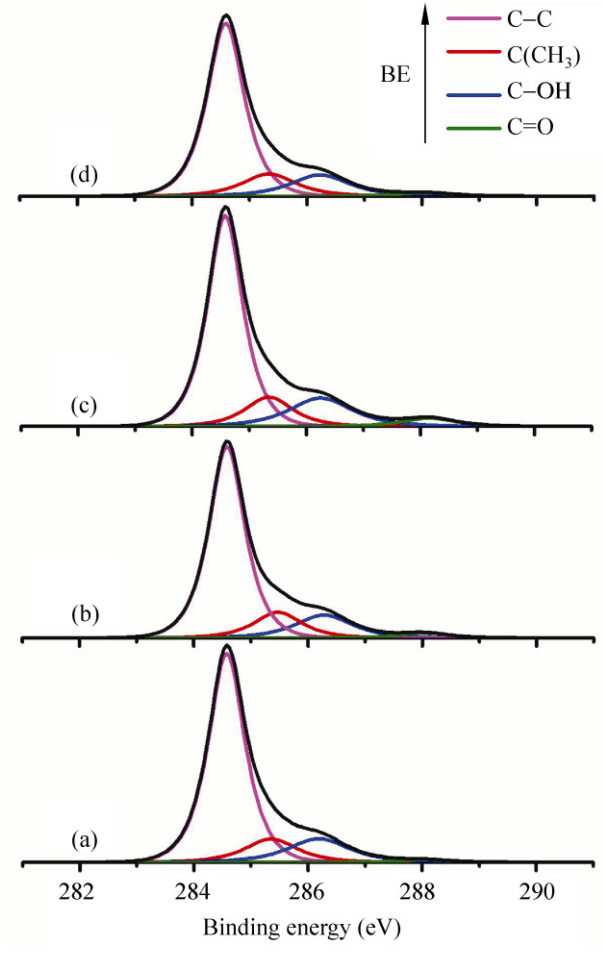

Figure S-3 Peak deconvolution of the C (1s) XPS core level of graphene irradiated with different irradiation doses of (a) 7×10^4 Gy, (b) 1.4×10^5 Gy, (c) 2.1×10^5 Gy, and (d) 2.8×10^5 Gy

Table S-1 The peak area (A) ratios of the oxygen-containing bonds to the C–C bonds, for graphene sheets before and after annealing

Sample	Graphene oxide sheets	After annealing
A_{COH}/A_{CC}	0.67	0.18
A_{CO}/A_{CC}	0.09	0.02

Table S-2 The peak area (A) ratios of the oxygen-containing bonds to the C–C bonds, for graphene irradiated with different irradiation doses

Irradiation dose	7×10^4 Gy	1.4×10^5 Gy	2.1×10^5 Gy	2.8×10^5 Gy
A_{COH}/A_{CC}	0.19	0.20	0.24	0.19
A_{CO}/A_{CC}	0.02	0.03	0.06	0.03